STATISTICAL TIME SERIES MODELS OF PILOT CONTROL WITH APPLICATIONS TO INSTRUMENT DISCRIMINATION

R. E. Altschul
P. M. Nagel
F. Oliver

The Boeing Company
Post Office Box 3707
Seattle, Washington 98124-2207

June 1984

INTRODUCTION

Advanced information displays have altered the way pilots interact with the airplane and the way they exercise control. Use of these displays inpacts the cognitive skills used to effect vehicle control in subtle ways. A method of modeling continuous human flight path control has been developed that has proved useful in understanding the effect of these displays on performance and in providing a more precise quantitative description of the pilot vehicle interaction. The method utilizes new technology in multivariate statistical time series for identifying and estimating multi-input/output transfer function models. It is completely data driven and does not depend on any prior knowledge of the system under consideration, but only on a definition of the loop being investigated in terms of the variables involved. Autoregressive moving average models are evaluated in the time domain using state space estimation techniques developed by H. Akaike (1). Once the models are identified, the observed process vector is regarded as the output of a linear system with a rational transfer function matrix subject to white noise input and considered in the frequency domain.

Models have been obtained for a variety of flight situations based on pilot-aircraft performance data obtained from a series of full mission flight simulations and tests in actual flight. One of the primary issues of concern during these tests was a comparison of overall pilot performance using a new flight deck MAP navigation display versus performance using the standard VOR direction indicator over several subjects. The methods used provided evidence to the effect that a pilot's continuous control was measureably different as a function of the navigation information display. They also proved useful in providing performance based quantitative measures for exploring pilot variablity and for comparing control strategies of individual pilots as they respond naturally to the varying demands of the flight path.

Although this study is far from complete, the paper includes:

(i) a general description of the methodology used in obtaining the transfer function models and verification of model fidelity,
(ii) frequency domain plots of the modeled transfer functions,
(iii) numerical results obtained from an analysis of poles and zeroes obtained from z plane to s-plane conversions of the transfer functions, and
(iv) the results of a study on the sequential introduction of other variables, both exogenous and endogenous into the loop.

EXPERIMENT

The analysis is based on a series of flight simulation experiments conducted over a period of months in 1981 in a 767 flight simulator in concert with a series of flight tests on an actual 767 airplane.

The simulations were conducted in the 767 Systems and Workload Display cab at the Renton Flight Simulation Facility of The Boeing Company. Although several flight scenarios were simulated, this analysis is based on a replica of a standard flight profile of a line operation night flight from Seattle to Moses Lake. All of the flight test measurements were obtained from flights over the same route in full daylight.

The objective of the tests was to obtain a workload data base that includes data on eye movement and fixation times, execution times for discrete, manual, verbal and auditory tasks and time traces of continuous control movement and aircraft attitude and flight condition measures. For the simulations the continuous data series were recorded on magnetic tape at a sampling rate of 6.41 per second (one every .156 seconds) and, for flight test, the sampling rate was 5.0 per second (one every 0.2 seconds).

Data was recorded for five pilot - copilot combinations for each of the simulations and for three crews in flight test. The study was designed to determine if two of the presentation formats of navigation information affect pilot control. Specifically, each crew flew two flights, one using the more conventional VOR display mode on the Electronic Horizontal Situation Indicator (EHSI) for navigation guidance throughout the flight and the other with the MAP mode displayed. Figure 1 compares the two display modes. Not all cases in the design resulted in a successful record, hence this analysis is based on a subset of comparable cases. In particular, there was only a single pilot-copilot combination that was common to both instrumentation conditions across both simulation and flight.

ANALYSIS TECHNIQUES

The analysis performed in this study is based on the general class of linear functions of sampled data systems represented by autoregressive moving average (ARMA) models of the form:

$$z(t) - A_1 z(t-1) - \ldots - A_p z(t-p) = e(t) + C_1 e(t-1) + \ldots + C_q e(t-q)$$

where $z(t)$ is the vector of the observed process, p and q are numbers representing the model structure, A and C are constant matrices and $e(t)$ is a vector of zero mean white noise Gaussian processes. The use of this ARMA model in the modeling of a single time series is extensively discussed by Box and Jenkins (2).When the series $z(t)$ and $e(t)$ are univariate processes, practical methods for estimating the matrices A and C and the structure identification parameters p and q are relatively recent. The extension of the application of ARMA models to

the analysis of multivariate time series where $z(t)$ is a set of possibly dependent variables is considerably more difficult particularly with regard to structure identification. In the last four to five years several computer codes have been written to perform this task, one of which is based on a method proposed by Akaike. See references (3 and 4) for more detail in addition to reference (1).

In a statistical estimation procedure an estimate is best if it fits optimally to a set of observed data relative to some criterion. Akaike extends this concept to include estimates of the statistical model identification parameters as well, namely, the parameters p and q. Therefore the performance of the model as well as the estimates of the free parameters of the model are influenced by the choice of criterion of model fit. The one proposed by Akaike minimizes an information criterion called AIC where:

$$\text{AIC} = -2(\log \text{likelihood}) + 2(\text{number of independent parameters})$$

and $$\text{MAICE} = \min(\text{AIC})$$

where the minimum is taken over all models of the candidate class. The model that attains the value of MAICE gives the final estimate.

Starting from the ARMA multivariate model in an equivalent canonical Markovian state space stochastic representation, Akaike has shown that the MAICE solution solves the problem of identifiability under very general conditions on the stochastic process.

The code used in this study is based on Akaike's methods of state space parameter identification as implemented in the Statistical Analysis System (SAS) general purpose time series analysis package procedure STATESPACE, reference (5). The state space model on which the code is based can be developed from equation (1) according to the following steps. By solving this equation iteratively for z in terms of e, the infinite series

$$z(t) = e(t) + D_1 e(t-1) + D_2 e(t-2) + \ldots , \quad D_0 = 1$$

is obtained. Denoting the conditional expectation (projection) of $z(t+i)$ on all the past history of z up to time t by $z(t+i|t)$, then:

$$z(t+i|t) = D_i\, e(t) + D_{i+1} e(t-1) + \ldots$$

and

$$z(t+i|t+1) = z(t+i|t) + D_{i-1}e(t+1)$$

Furthermore from Equation (1):

$$z(t+r|t) = A_1 z(t+r-1|t) + \ldots + A_r z(t).$$

where $r = \max(p, q+1)$

These equations can then be summarized in the following form:

$$\begin{bmatrix} z(t+1) \\ z(t+2|t+1) \\ \cdot\ \cdot\ \cdot\ \cdot\ \cdot \\ z(t+r|t+1) \end{bmatrix} = \begin{bmatrix} 0 & 1 & 0 & \ldots & 0 \\ 0 & 0 & 1 & \ldots & 0 \\ \cdot & \cdot & \cdot & \cdot\ \cdot\ \cdot\ \cdot & \\ A_p & A_{p-1} & A_{p-2} & \ldots & A_1 \end{bmatrix} \begin{bmatrix} z(t) \\ z(t+1|t) \\ \cdot\ \cdot\ \cdot\ \cdot \\ z(t+r-1|t) \end{bmatrix} + \begin{bmatrix} 1 \\ D_1 \\ \cdot \\ D_{r-1} \end{bmatrix} e(t+1)$$

or $v(t+1) = Fv(t) + Ge(t+1)$

Since the state vector $v(t)$ is comprised of conditional expectations of $z(\cdot)$ and its first components are $z(t)$, it allows for the representation

$$z(t) = H\,v(t) \text{ where } H = \begin{bmatrix} I & 0 \end{bmatrix}.$$

In summary therefore:

$$\begin{aligned} v(t+1) &= Fv(t) + Ge(t+1) \\ z(t) &= Hv(t) \end{aligned} \qquad (2)$$

which is the Markovian state space representation of the ARMA model (1).

Starting with the ARMA model in the form of (2), the objective of Akaike's method is to compute the maximum likelihood estimates of the free parameters of a given model and then select that model which gives a minimum value of AIC. Although the objective is simple to describe, most implementations are time consuming and potentially unstable. All depend on the choice of an appropriate initial value for success. The SAS implementation uses a method recommended by Akaike. The method proceeds by first fitting an AR model to the observed series by solving a sequence of Yule Walker equations. A final order, M, is then selected that minimizes the AIC information criterion. This order is then used as the number of lags into the past in a canonical correlation analysis that searches for linear

dependence among the linear predictors of the future z(t), z(t+1), ... based on a finite number of past observations z(t), z(t-1), ..., z(t-m). The algorithm proceeds sequentially, successively adding new components, z(t+i), until the canonical correlations are no longer significant. The importance of the correlation associated with the additon of a new component is judged according to another information criterion. This analysis also provides an initial estimate of the remaining free model parameters as well as an initial estimate of the innovation variance-covariance matrix. These values are input to a nonlinear optimization procedure that calculates final estimates of the model parameters based on an approximate maximum likelihood procedure.

If the process converges, the procedure supplies an estimate of the model in statespace form (2), and a covariance matrix for the innovation process e(t). Forecasts and residual plots are also obtainable. The ARMA form of the model is then retrievable by reversing the steps outlined above. Software has been developed for this procedure and is available in SAS.

Once the model is identified, z(t) can be regarded as the output of a linear system with a rational transfer function K(ω) subjected to a white noise input. See e.g. Priestly (6). The transfer function matrix has the form

$$K(\omega) = A(\omega)^{-1}C(\omega) \tag{3}$$

where

$$A(\omega) = I + A_1 e^{-i\omega} + \ldots + A_p e^{-i\omega p} \tag{4}$$

and

$$C(\omega) = I + C_1 e^{-i\omega} + \ldots + C_q e^{-i\omega q} \tag{5}$$

for the matrices A_i and C_i defined in (1).

If Σ is the variance covariance matrix of the innovation process e(t), then the spectral matrix F of the process Z is given by

$$F(\omega) = K(\omega)\Sigma^{-1}K^{*}(\omega) \tag{6}$$

where K^{*} = conjugate transpose of K .

For the two dimensional closed loop system representation of Figure 2 (a) with open loop representations (b) and (c), let z = (x, y). Then, analytically, the two, open loop, input-output representations become:

$$x(t) = \sum_{0}^{\infty} j(u)y(t-u) + V(t)$$

and

$$y(t) = \sum_{0}^{\infty} h(u)x(t-u) + N(t)$$

where

$$J(\omega) = \sum_{-\infty}^{\infty} j(u)\exp(-i\omega u)$$

is the transfer function at A and

$$H(\omega) = \Sigma h(u)\exp(-i\omega u)$$

is the transfer function at B. If, for this case, the matrices A and C of equations (4) and (5) have elements $a_{ij}(\omega)$ and $c_{ij}(\omega)$, respectively, then the transfer functions J and H are estimated from:

$$J = (a_{11}c_{22}-a_{21}c_{12})^{-1}(a_{22}c_{12}-a_{12}c_{22}) \tag{7}$$

$$H = (a_{22}c_{11}-a_{12}c_{21})^{-1}(a_{11}c_{21}-a_{21}c_{11}) \tag{8}$$

and the noise filters $S(\omega)$ and $R(\omega)$ corresponding to the outputs N(t) and V(t), respectively, from

$$S = (a_{22}c_{11}-a_{12}c_{21})^{-1}(c_{11}c_{22}-c_{12}c_{21})$$

$$R = (a_{11}c_{23}-a_{21}c_{12})^{-1}(c_{11}c_{22}-c_{12}c_{21}).$$

Note that J, H, S and R are rational functions. In general, ARMA models lead to rational functions in the frequency domain. See e.g. Priestly (6).
For two dimensional loops, procedures have been written for plotting the transfer functions J, H, S and R both amplitude and phase, modeled spectra for X, Y, V and N and the corresponding coherency spectra. Three and four dimensional models have also been considered although not all of the above software has been developed for all cases.

Although the use of the SAS code appears to be nearly automatic, there are several decision points in the process that make model fitting at this time take on some of the characteristics of a subjective process. The primary decision has to do with loop definitions: what variables should be included and what the consequences are of leaving variables out, what

interdependent structure exists and whether there are subloops with special structures; whether the subloops should be modeled as a suboptimization conducted prior to the final modeling exercise, what variables are exogenous and how they should be modeled; should the variables be detrended and how nonstationarity should be treated.

Other decisions are a consequence of the evaluation process after models are produced. The MAICE procedure is consistent with the principle of parsimony. That is, increasing the number of parameters in a model has an adverse effect on the minimum unless the increase is balanced with an equivalent increase in the likelihood. Thus this procedure has a definite tendency to converge on models with small values of the identification parameter, that is small values of p and q. It is therefore advantageous at times to force other model orders into consideration after the initial values of the innovation matrix or the residuals indicate an ill fitting model in some respect. Usually the immediate neighborhood of the fitted parameter was searched for improvement.

The STATESPACE procedure can be used in a mode that prespecifies a particular model for a given time series or particular values for the identification parameters. In this way the user of the program can exercise a significant degree of control and guidance over the nature of the subsequent convergence.

APPLICATION AND VALIDATION

The characteristics of a human operator cannot be put into a single class. Over time the human controller of an aircraft displays a wide variety of control behavior: linear, nonlinear, time varying, and adaptive, with varying degrees of randomness in the control. The controller can act as a servo in response to various information sources in the flight deck or can respond by acting upon information or internal motivation from outside the control loop. Therefore, since no single model of human control can be completely comprehensive, the hypothesis of the model building of this study is that valid models can exist for restricted classes over relatively short time periods.

Model development has proceeded on the climb portions of the simulations and flight test from a few seconds after rotation to cruise altitude. For each test condition plots of altitude, airspeed and heading were examined and comparable time periods of approximately one and one-half minutes were selected across the five pilots at various points along the flight path. These periods formed the basic data set for this part of the study.

Since this study is based entirely on a black box look at both the pilot and the vehicle, four graphs from an earlier study are included in Figure 3 that provided insight into the nature of pilot-instrument interaction, pilot to pilot variations and within pilot variation in strategy as the goals of the flight plan are executed. Figures 3 (a) and (b) superimpose the estimated raw spectral densities of aircraft pitch, the displayed aircraft pitch command on the flight director, and the corresponding pilot

column performance. Figures 4(c) and (d) are similar graphs for roll and wheel. The graphs are for two pilots and at a high level of wind turbulence. In all cases the displayed information has a band width that is broader than the corresponding aircraft response and is encouraging a response in the pilots that is broader in band width. Pilot A has matched his response fairly carefully to the indicator but pilot B has a much noisier response that seems to have been propagated by the noise in the indicator. In all cases the pilots seem to be working harder than necessary caused to a degree by the displayed information. The flight director information was not available to the pilot in any of the subsequent experiments.

Figure 4 provides graphs of wheel and column standard deviation for three pilots computed over one and one-half minute intervals at various positions during climb. The data was gathered during an experiment in a flight simulator conducted prior to the one described in the previous section. The subjects were instructed to climb to 31,000 feet in three stages: first, climb to 5,000 feet while making a heading change of 140 degrees, second, climb to 10,000 feet while making a heading change of 100, and third, climb to 31,000 feet turning 20 degrees just before level off. The series have been aligned vertically by the time of rotation. These graphs illustrate clearly the degree of similarity in pilot performance when executing similar tasks and that a pilot's performance varies widely as the task changes. Indeed, for these pilots, there is more variation in a pilot's performance due to changes along the flight path strategy than there is between pilots at any given time or comparable flight condition.

Since this paper is primarily related to display related pilot responses the data sets that are discussed are those comparing:

pilot to pilot variation in control behavior,
pilot variation and navigation display mode (MAP versus VOR),
pilot variation during climb along the flight path,
navigation display mode usage during climb, and
pilot control performance during simulation and actual flight.

Subsets of the basic data set have been selected for making these comparisons and models fitted based on the SAS/STATESPACE procedure. In most cases the modeling process was based upon the control loop structure illustrated in Figure 2 with H as the human transfer function and J that of the aircraft. Since navigation display mode was thought to influence lateral control more than vertical, the initial study was conducted on a loop defined by $x(t)$ = aircraft roll response and $y(t)$ = pilot wheel control response with $N(t)$ as the pilot residual and $V(t)$ as the aircraft residual. A later study, performed on a loop defined by column control and airplane pitch response, was extended systematically to include other variables. For the current study, however, it did not seem necessary to do so, although for a complete understanding of pilot response it is essential.

Wind turbulence is the disturbing force in the loop and would have been used in defining the loop had it been recorded in flight. Since it was not available for the flight tests, the variable was not used in the results presented here and its effect was presumed to affect the pilot only in terms of the roll variable. The lack of this variable distorted the aircraft residual and reduced precision in the loop but did not seriously effect pilot gain.

Box and Jenkins (2) discuss differencing as a method of removing trend and achieving stationarity in a sampled series. On occasion it seemed necessary to do this in one or more of the observed series. As the simulator model of the aircraft developed over time, however, it became less and less necessary, and the current models are based on the original observed data series.

Several tests, both quantitative and subjective, were applied to a model before it was considered acceptable. As a first step, the modeled innovation variance-covariance matrix was examined. For acceptance the entries had to be small relative to the observed series. Convergence itself demonstrated that there was sufficient information in the defined loop, and that the model used by the pilot in that time frame was sufficiently stable to produce a model. This was not always the case. Lack of convergence sometimes occurred and was usually of two types. During dynamic periods with large control inputs on the part of the pilot, convergence was often achieved by sliding the time unit slightly. This indicated a very dynamic change in model with time such that a badly chosen time frame might span two or more separate models. During the least dynamic part of the climb, about midclimb, convergence was also sometimes difficult to achieve. During this period, the pilot seemed to have achieved the desired stability in the flight dynamic variables and was acting more in the capacity of an instrument monitor rather than a linear processor. This was also the case after level off at cruising altitude.

STATISTICAL GOODNESS OF FIT

Statistical goodness of fit tests were performed on the model residuals. The Bartlett's Kolmogorov-Smirnov white noise test was performed on both residuals and only those series passing both tests at the 5 percent level were accepted. SAS made it also possible to plot model residuals against the observed series for visual inspection of the effects of model fitting. In general, the residuals were very small and had the characteristics of white noise. The largest deviations from the observed series occurred primarily when the first differences of the series were large such as, after a period of relative stability in control movement. In figure 5 are residual plots for roll and wheel, respectively, for a typical case of model development.

The subjective elements of model validation has to do primarily with prior expectations regarding the nature of the models themselves. One of the first things that was checked was the stability of the aircraft model across pilot and, to a degree, across flight conditions. Though not known in advance, the resultant equations did display the required model con-

stancy. The pilot models on the other hand, did not; a result which was also expected. The pilot models did, however, exhibit expected trends with flight path.

Integrating the modeled output spectral densities computed from equation (3), produced values for the variances of the modeled series which were then compared to the original sample variances computed from the raw data series. Table 1 compares these estimates in terms of standard deviation for the models discussed in this paper. Models for simulation are much closer, as expected, than those for flight with respect to this measure. In flight the roll percentage differences average 5.9 percent compared to .7 percent in simulation and for wheel the percentages are 2.4 and .7, respectively.

Figures 6 and 7 superimpose the model based spectral densities on the estimated densities calculated from the raw data series. In general, the modeled spectral density is much smoother and has a broader band width than the raw data spectrum and without noticeable peaks and valleys reflecting the overall parsimony of the fitted equations. In every case but one, the fitted spectra track the raw spectra very closely in overall features. For the one case, the low frequency aircraft response is badly modeled and should have perhaps been filtered by a difference filter to improve the modeling.

When convergence was not achieved on the innovations or the residual variances were too high for a model to be acceptable, alternatives were explored. The data series were often shifted by ten to twenty data points at either end in an attempt at locating a fixed model rather than one in transition. A high pass difference filter was also used, though somewhat sparingly, as a device to improve model fit. Other segments were set aside to be investigated in conjunction with larger loop definitions.

These results verify the fidelity of statistical time series techniques applied to the problem of modeling pilot control performance. Good quantitative models of the pilot exercising his control task can be produced that have both statistical and physical validity. The next question then, is to determine what they say about the pilot and how they can be used to provide insight into the control process.

RESULTS

There are thirty-nine modeled flight segments in all, a subset of which are represented in Table 2. The segments consist of twenty-six from the simulation results and thirteen from the results in the aircraft. Of the simulated flight segments, ten are from a flight segment common to each of five pilots flying once with the VOR navigation display and again with the MAP navigation display. The other sixteen simulated flight segments consist of nine VOR and seven MAP segments flown by a single pilot. The thirteen aircraft flight segments consist of five VOR and eight MAP segments all flown by this same pilot. The models are closed loop roll-wheel models, corresponding to Figure 1 for the original roll signal

Most of the control literature on the human transfer function is in terms of a continuous control function, and for this reason the z domain transfer function was transformed into the s domain. Since the z-domain transfer function is a rational function, it can be written as a partial sum:

$$H(z) = \sum_{i=1}^{m} A_i/(1-e^{-s_i T} z^{-1})$$

where m is the number of poles, T is the sampling interval and $z = e^{i\omega T}$. Using the correspondence:

$$H(z) = \sum_{i=1}^{M} A_i/(1-e^{-s_i T} z^{-1}) \longrightarrow \sum_{i=1}^{M} \frac{B_i}{s+s_i} = Y(s)$$

the general form of the pilot transfer function is still a rational function:

$$Y(s) = Ke^{-Ts} \Pi(s+z_i)/ \Pi(s+p_i)$$

where K is pure gain and the z_i's and p_i's are the zeroes and poles of Y, respectively. The use of this correspondence in human operator control modeling also appears in Shinners (9) and Osafo-Charles (10).

The z_i's and p_i's are not always real numbers but frequently occur as complex pairs causing second order factors in the numerator and denominator. The complex poles are more likely to be the two smallest in simulation and the two largest in flight. Complex zeroes are not nearly as frequent. Writing the complex term in the denominator as

$$[(s+(a+bi)][(s+(a-bi)] = \omega^2(s^2/\omega^2+2\zeta s/\omega+1)$$

where ζ = damping ratio

and ω = normalization frequency

The damping ratio was computed for the models developed for the one pilot flying both in the simulator and in actual flight. In the simulator, of the eleven models with second order poles, ζ ranged from .41 to .98 with approximately two thirds of the ratios above .71. For flight the situation was somewhat reversed; of the nine models with second order poles, one was above .71, one at .71, and the rest were below.

sampled at the display mode and the original wheel signal. Neither signal has been filtered.

Graphs of the modeled pilot roll to wheel transfer functions are given in Figures 8 and 9. The graphs cover small flight segments for a single pilot, flying in actual flight, covering a total time span from rotation to cruise altitude. Two flights are represented with different display modes. The graphs are plotted in the z domain using formula (8). The functions are typical of those published by other authors. See e.g., Tanaka (7) and Shirley (8).

The similarity in control exercised by the pilot over comparable time periods between the two flights is worth noting. This is obviously related to the similarity in flight goals during comparable periods of different flights. The dissimilarity of models along the time axis is a measure of the variety of strategy required of the pilot in achieving these goals.

Some thought has been given to the concept of pilot remnant relative to the pilot models developed for these series. Since the concept was originally defined in an open loop context, there is some confusion as to its meaning when the loop is closed. Several authors have defined remnant in terms such as "that part of the output not related to the forcing function" or as "that part of the output not correlated with the input." In closed loop time series modeling the only term of the ARMA time function satisfying this concept is the pilot innovation.

This can be made more explicit, by writing the ARMA model for the pilot in the form:

$$\theta(B)y(t) = \phi(B)x(t) + \beta(t) + \gamma(B)B\beta(t) + \delta(B)B\alpha(t) \qquad (9)$$

where B is the backward shift operator defined by

$$Bx(t) = x(t-1)$$

and θ, ϕ, γ and δ are polynomials in B. Since $\beta(t)$ is white noise it is independent of its own past. $\alpha(t)$ and $\beta(t)$ are contemporaneously dependent only. Therefore $\beta(t)$ is independent of the γ and δ terms of equation (9). $x(t)$ depends only on the past history of $\beta(t)$ and not on its present or future, hence $\beta(t)$ is also independent of the ϕ term.

Often the last three terms of equation 9′ are combined into a single remnant term $N(t)$. Not only is this term correlated both with the input series x and both innovation series, it also has more information in it than the concept of remnant usually implies. In particular, in its final form, the transfer function associated with the pilot's innovation series $\beta(t)$ seems to represent the pilot's compensation based on his memory of past "remnants." Although, this term has not yet been studied in detail, it could provide some interesting information on the pilot's cognitive process.

Table 3 summarizes the differences in the poles and zeroes of the pilot's describing function when using the two navigation information display modes for a single flight segment across five of the six pilots who participated in the simulation test. The segment was 90 seconds in duration and a careful attempt was made to match flight conditions across all five pilots even though not all pilots encountered the same conditions at the same time in flight. Pilot control was tapped approximately seven and one-half minutes into flight when the altitude was 14,700-16,700 ft, heading 68.5^{o}-69^{o}, and airspeed approximately 300 knots. But, even though this criterion was somewhat fuzzy in definition, three of the five pilots demonstrated very similar control behavior.

If the complex zeroes and poles are replaced by their corresponding absolute values, this data suggests certain tentative hypotheses:

a) The second zero is usually very large and can be ignored as it has little effect on the frequencies of interest.

b) The time constant associated with the largest pole is measuring an aspect of the pilot's response delay. The time is nearly constant over all of the conditions and averages .126 seconds with a standard deviation of .025.

c) The control lead time constants associated with the first zero are longer using the MAP display than for VOR.

d) The control lag time constants as measured by the first pole are generally shorter when using the MAP display although this effect is not as pronounced as the lead time effect.

e) Pilot equalization as measured by the ratio of the first zero to the first pole is generally less than one for pilots using the MAP display and greater than one for the VOR display.

Thus, in effect, by introducing the MAP display the pilots are demonstrating higher lead times with less lag than their performance using the VOR display. The general positive acceptance of the MAP display obtained from pilots in debriefings implies that this result has been achieved without an adverse effect on pilot workload.

In order to determine if these results were particular to the flight conditions and control strategy in effect at the time selected for analysis, pilot control strategies at several different time segments during the climb phase were investigated. The investigation was conducted on data from both simulation and actual flight for the one pilot flying both models. Figure 10 summarizes the definition of the selected segments in terms of the flight condition measures: heading, airspeed and altitude. Pilot control strategies for these segments were analyzed in terms of the poles and zeroes of the transfer function in the canonical form for both MAP and VOR navigation display modes.

Figure 11 contains graphs of the first zero and first pole, as a function of time into flight from rotation, for the simulation experiment's MAP and VOR mode results. Each plotted point represents a time interval of approximately 90 seconds. Since the VOR zeroes dominate the MAP zeroes, the MAP lead time constants are longer than VOR which substantiates the previous results. The MAP poles are larger in general than the VOR poles though not as consistently. This too substantiates the previous results.

There is a substantial change in lead and lag time constants as a function of time into flight. As the climb progresses the pilot has less to do; flight path variation in performance decreases, lead and lag time constants decrease and the aircraft flight control stabilizes. As cruise altitude is reached, the strategy changes: performance variation increases and the lead and lag time constants increase. The pilot is adapting performance behavior to fit the control task.

Figure 12 portrays a similar scenario for the experiment involving actual flight. MAP zeroes are generally less than VOR zeroes making MAP lead time constants larger. MAP poles are generally greater than VOR poles making VOR lag time constants greater than MAP. The trend with time into flight is also evident with the lead time constants generally larger when the flight control goals are more dynamic.

By comparing the scales of Figures 11 and 12 it can be determined that the simulation zeroes are for the most part larger than those for actual flight. A similar determination is also possible for the poles. Thus, in general, the lead and lag time constants are both smaller for simulation than flight which implies that the flight simulator requires less lead input from the pilot for control compared to actual flight and lags less.

Figure 13 is a graph of the pilot equalization ratio in order to determine if the control is dominated primarily by lags or by leads over the lower end of the frequency band. All four test conditions are superimposed. In general, this graph shows that, except for the MAP condition in simulation, pilots generally lag more with VOR than with the MAP navigation display and more in flight than in simulation. In both the simulator and in actual flight the MAP display results shows a significant decrease in the equalization ratio.

In these models, as in those represented in Table 3, there is a relatively high frequency pole representing pilot response time. During simulation the average was .15 seconds or slightly larger than the average for Table 3, due to a wider variety of flight conditions. For flight the average is .25 seconds. The degree to which these results are confounded with the sampling rate is not known.

MULTI-INPUT, MULTI-OUTPUT PILOT CONTROL MODELS

A cursory investigation was conducted to explore the effect of removing the lateral component of the wind turbulence vector, v_g, from the roll

wheel simulation models of the previous section. The investigation was performed on a single time interval from a simulated flight of 70 seconds, starting approximately 5 minutes into flight. As wind is an exogenous variable, a univariate ARMA model was fit to the time series of the lateral wind component prior to formulating the problem as a multivariate statespace model. This ARMA model was then introduced into the statespace model and remained unchanged during the remainder of the model fitting process. The final model indicates, as expected, that roll has a strong dependence on v_g but that the wheel dependence on v_g is very weak. Figure 14(a) is the power spectrum of the model residuals between the one step ahead forecast and the observed data for wheel. There was no visible difference before and after v_g was introduced. The same comparison is made for roll in Figures 14(b) and (c). The change in the roll spectrum, however, clearly demonstrates that much of the lack of model fit for the lateral variable is directly attributable to this component of wind. The pilot's response to wind is almost completely through the roll variable whereas the aircraft's response is direct. Figure 14 (d) is a time history of the roll residual after v_g was introducted superimposed on the observed roll series. Comparing this plot to the residual in figure 5 for the same case before v_g was introduced, clearly demonstrates that the fit improvement is both in amplitude and over the low frequency part of the spectrum.

A second study of the effect of adding more variables in the loop was performed on a loop that initially involved just the pitch and column variables where pitch was differenced for trend removal. The variables airspeed and the vertical component of wind turbulence w_g were then added sequentially to the model. As before, a univariate ARMA model was fit to the wind component and then added to the statespace model as an exogenous variable.

Figure 15 gives the results of sequentially adding variables to the defined loop as they affect the pilot transfer of the differenced pitch signal. The lowest curve is the pilot transfer of the differenced pitch signal with no other variables in the model. The middle curve is the same transfer function but with airspeed added to the model. The increased pilot gain is frequency selective over the lower frequencies. The upper curve represents the addition of w_g to the model. Again, the added variable is frequency selective affecting only the higher frequencies.

CONCLUSION

This approach seems to have general application as a human factor design aid in display development with regard to such characteristics as the selection of format and information content, the placement and integration of displays, the selection of color/contrast and brightness levels, etc. It is based on minimal model assumptions of linearity and "optimality" of performance. The results not only have provided quantitative measures that have discriminated between display modes, but seem also to have objectively quantified some of the cognitive features of pilot workload. Indeed, its real value as an analysis tool seems to be its sensitivity to the natural control choice of the pilot at the time it is made, as opposed to having to rely on information gained from intrusive measuring devices to understand this process, or having to evaluate mission performance as a whole in terms of arbitrary success criteria or subjective debriefings.

The method does not appear to be limited to continuous performance models. An investigation has already been initiated in applying statistical time series methods to model the pilot as a supervisor or monitor of states combining visual clues with control movements.

Because the method depends on information obtained from expensive simulation, it does not replace other methods currently in use to predict and design information systems. Instead it can be used to complement this activity, e.g., as a research tool to confirm the applicability of these methods or to develop them further with a better understanding of their strengths and weaknesses. The methods of this paper can also be used after the fact, that is, after initial design decisions have been implemented, to fine tune the displays and control system parameters that involve pilot input. Finally, the methods can provide a better understanding of the job of piloting aircraft: in quantifying variation within pilots, in quantifying the interplay of the information variables and the corresponding control, and in quantifying the variation in control and the use of information as a function of the resultant maneuver.

References

1. Akaike, H. "Canonical Correlations Analysis of Time Series and the Use of an Information Criterion." In R. Mehra and D. G. Lainiotis (eds.), Advances and Case Studies in System Identification. New York Academic Press, 1976.

2. Box, G.E.P., and Jenkins, G. Time Series Analysis: Forecasting and Control. Holden Day, 1976.

3. Akaike, H. "Markovian Representation of Stochastic Processes and its Application to the Analysis of Autoregressive Moving Average Processes." Annals of The Institute of Statistical Mathematics, 26: (1974), pp. 363-387.

4. Akaike, H. "On the Identification of State Space Models and Their Use in Control." In D. R. Brillinger and G. C. Tiao (eds.), Directions in Time Series. Proceedings of the IMS Special Topics Meeting on Time Series Analysis. Iowa State University, Ames, Iowa, May 1978.

5. SAS/ETS User's Guide: Econometric and Time Series Library, 1982 Edition, SAS Institute, Cary, North Carolina.

6. Priestly, M. B., Spectral Analysis and Time Series Vol. I and II, Academic Press, 1981.

7. Tanaka, K., Gato, N. and Washizu, K. "A Comparison of Techniques for Identifying Human Operator Dynamics Utilizing Time Series Analysis" Proc. Twelfth Annual Conf. on Manual Control, NASA TM X-73170, pp. 673-693, 1976.

8. Shirley, R. S., "A Comparison of Techniques for Measuring Human Operator Frequency Responses" Proc. Sixth Annual Conference on Manual Control, AFFDL, pp. 803-869, April 1970.

9. Shinners, Stanley M. "Modeling of Human Operator Performance Utilizing Time Series Analysis," IEEE Transactions on Systems, Man and Cybernetics, Vol SMC-4, No. 5, pp. 446-458, September 1974.

10. Osafo-Charles, Frank; Agarwall, Cyan C.; O'Neill, W. D. and Gottlieb, Gerald L. Application of Time-Series Modeling to Human Operator Dynamics," IEEE Transactions on Systems, Man, and Cybernetics, Vol. SMC-10, No. 12, pp. 849-860, December 1980.

		ROLL			WHEEL		
	TIME (SEC.)	Observed	Modeled	% DIFFERENCE	Observed	Modeled	% DIFF
SIMULATION	MAP						
	360-450	4.371	4.391	0.4	3.887	3.887	0.0
	450-540	6.049	6.339	4.8	2.752	2.746	0.2
	540-630	1.561	1.561	0.0	1.538	1.538	0.0
	630-720	1.298	1.299	0.08	1.106	1.106	0.0
	730-790	0.992	0.992	0.0	0.849	0.849	0.0
	800-890	1.383	1.383	0.0	1.728	1.728	0.0
	980-1070	1.742	1.743	0.0	1.661	1.661	0.0
	VOR						
	110-200	13.871	14.527	4.7	4.729	4.707	0.5
	200-290	11.060	11.127	0.6	4.269	3.850	9.8
	300-370	1.699	1.699	0.0	2.302	2.302	0.0
	380-470	2.924	2.924	0.0	2.699	2.699	0.0
	470-560	2.579	2.579	0.0	1.938	1.938	0.0
	560-650	2.281	2.282	0.04	2.074	2.074	0.0
	650-740	3.466	3.465	0.03	2.451	2.451	0.0
	740-830	1.193	1.193	0.0	0.961	0.961	0.0
	830-920	3.566	3.566	0.0	2.991	2.990	0.03
FLIGHT	MAP						
	90-180	8.656	9.446	9.1	4.936	4.922	0.3
	180-250	11.491	10.806	8.4	3.396	3.079	9.3
	270-360	9.557	9.838	2.9	2.719	2.566	5.6
	340-400	2.277	2.340	2.8	1.521	1.517	0.3
	450-540	0.857	0.913	6.5	0.870	0.896	3.0
	540-630	0.739	0.738	0.1	0.656	0.655	0.2
	630-720	2.151	2.196	2.1	1.144	1.168	2.1
	720-810	1.677	1.731	3.2	1.075	1.079	0.4
	VOR						
	90-180	9.043	10.905	20.6	4.256	4.288	0.8
	180-270	8.829	9.218	4.4	2.309	2.287	1.0
	270-360	9.857	10.027	1.7	2.154	2.138	0.7
	360-450	0.927	0.958	3.3	1.008	1.012	0.4
	630-720	0.544	0.608	11.8	0.373	0.400	7.2

TABLE 1 Modeled and Observed Standard Deviation Comparison: Simulation (Top) and Flight (Bottom)

		COEFFICIENT									
	TIME	a_1	a_2	a_3	b_1	b_2	b_3	r_1	r_2	s_1	s_2
SIMULATION		MAP									
	360-450	-1.251	0.252		-1.420	1.390		0.328		1.084	
	450-540	-1.249	0.232		-1.100	1.087		0.335		1.246	
	540-630	-1.218	0.325		-0.360	0.272		0.111		0.509	
	630-720	-1.547	0.639		-0.202	0.158		-0.389		0.537	
	730-790	-1.212	0.496		0.516	-0.632		-0.366		-0.505	
	800-890	-1.427	0.542		-0.076	-0.024		-0.075		0.157	
		VOR									
	110-200	-1.440	0.474		-0.347	0.342		0.292		0.342	
	200-290	-1.347	0.404		0.00	-0.012		0.326		-0.044	
	300-370	-1.139	0.313		-0.034	-0.138		0.284		0.221	
	380-470	-1.464	0.878	-0.359	0.00	-0.505	0.554	0.129	0.195	-0.064	0.558
	470-560	-1.078	0.179		0.217	-0.263		0.263		-0.187	
	560-650	-1.442	0.316	0.186	0.00	0.339	-0.069	-0.329	-0.324	-0.157	0.052
	650-740	-1.369	0.152		-0.101	0.075		0.114		0.254	
	740-830	-1.074	0.345		0.273	-0.336		0.115		-0.263	
	830-920	-1.161	0.254		-0.049	0.003		0.450		0.027	
FLIGHT		MAP									
	90-180	-1.270	0.447		0.610	-0.606		0.069		-0.644	
	180-250	-1.265	0.285		0.00	-0.305		0.413		-0.106	
	270-360	-2.049	1.522	-0.461	0.00	0.00	-0.002	-0.481	0.045	0.029	-0.010
	340-400	-1.146	0.277		0.00	-0.043		0.272		0.206	
	450-540	-1.239	0.498		1.681	-1.769		0.230		-2.007	
	540-630	-1.259	0.537		1.195	-1.263		0.200		-1.483	
	630-720	-1.158	0.303		1.330	-1.335		0.441		-1.282	
	720-810	-0.397	0.076		0.227	-0.263		0.396		-0.236	
		VOR									
	90-180	-1.548	0.785		2.479	-2.481		-0.082		-2.651	
	180-270	-2.214	1.782	-0.548	0.00	0.00	-0.003	-0.799	0.032	-0.394	0.071
	270-360	-1.903	1.263	-0.337	0.00	0.00	-0.003	-0.355	-0.178	0.322	-0.009
	360-450	-1.203	0.324		0.481	-0.515		0.360		-0.551	
	630-720	-0.787	0.222		4.496	-4.497		0.443		-4.511	

Model: $y_t + a_1 y_{t-1} + a_2 y_{t-2} + a_3 y_{t-3} = b_1 x_{t-1} + b_2 x_{t-2} + b_3 x_{t-3} + \beta_t + r_1 \beta_{t-1} + s_1 \beta_{t-1} + s_2 \alpha_{t-2}$

TABLE 2 ARMA Coefficients Wheel (y) Output vs. Roll (x) Input, Wheel Innovation (β), Roll Innovation (α)

CREW-PILOT		MAP		EQUALI-ZATION	VOR			EQUALI-ZATION
1 - 1	ZERO	1.59		4.18	3.21	25.79		1.01
	TIME CONSTANT	0.63			0.311			
	POLE/MODULUS	0.38	6.17		1.89±2.55i/3.17	9.89		
	TIME CONSTANT	2.63	0.162		0.315	0.101		
3 - 5	ZERO	0.25	1.48	0.16	0.90	20.20		0.63
	TIME CONSTANT	4.00						
	POLE/MODULUS	1.13±1.11i/1.58	6.61±4.64i/8.08		1.43	7.35±0.86i/7.39		
	TIME CONSTANT	0.633	0.124		0.699	0.135		
4 - 7	ZERO	1.61	66.72	0.37	2.62	6.39		3.54
	TIME CONSTANT	0.621			0.382			
	POLE/MODULUS	2.42±3.57i/4.31	11.55		0.74	3.30	9.52	
	TIME CONSTANT	0.232	0.087		1.35		0.105	
5 - 9	ZERO	1.72	21.61	0.52	-3.02±5.40i/6.19			6.95
	TIME CONSTANT	0.581			0.162			
	POLE/MODULUS	2.79±1.79i/3.31	7.55		0.89	7.59±0.74i/7.62		
	TIME CONSTANT	0.302	0.132		1.12	0.131		
6 - 11	ZERO	0.84	∞	0.33	4.01	∞		1.50
	TIME CONSTANT	1.19			0.249			
	POLE/MODULUS	1.87±1.68i/2.51	8.53		0.96±2.50i/2.68	6.16		
	TIME CONSTANT	0.398	0.117		0.373	0.162		

TABLE 3 Wheel Model Poles and Zeroes of five pilots approximately 7½ minutes into flight, 300 KN airspeed, 68.5° - 69.5° heading, and 14,700 - 16,700 feet altitude. Roll-wheel loop.

VOR/ILS Mode – Partial Compass Rose – Heading Up

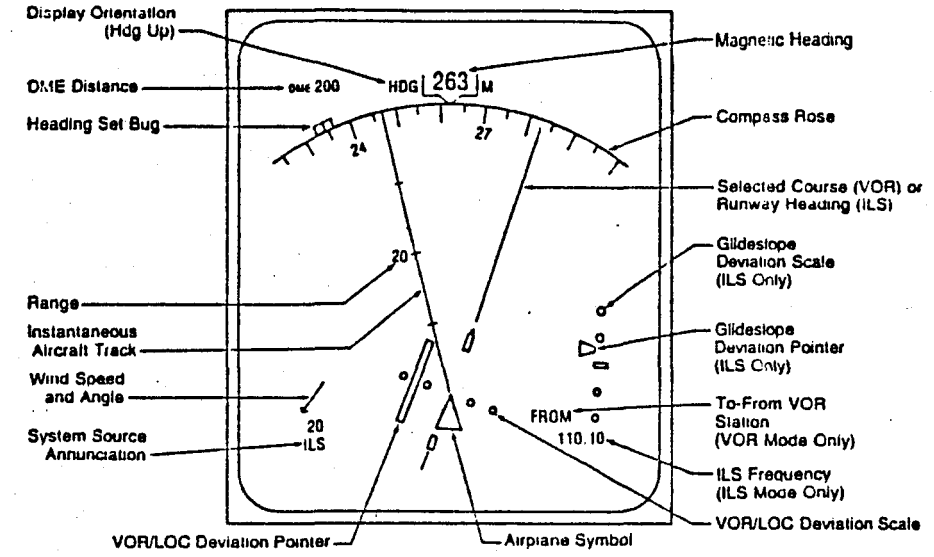

(a)

Map Mode – Track Up

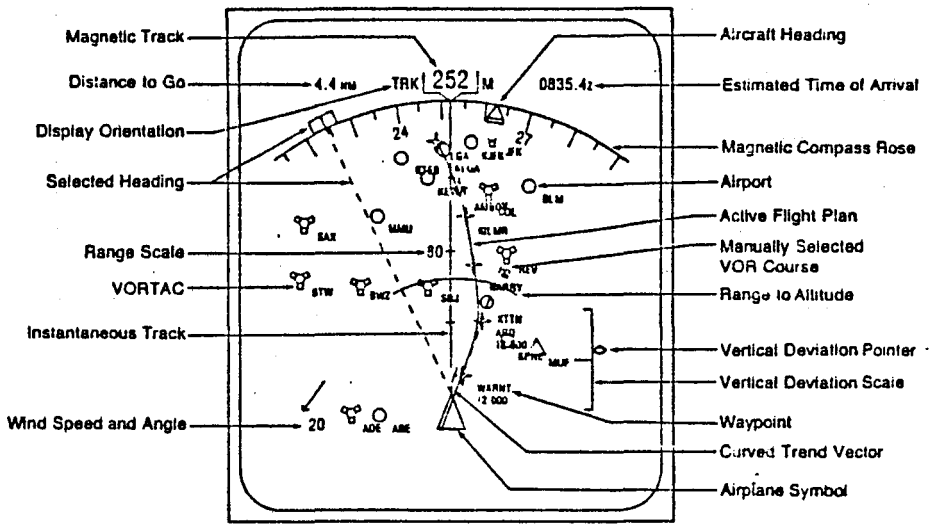

(b)

Figure 1 Horizontal Situation Indicator showing VOR/ILS Navigation Mode (a) and Map Mode (b)

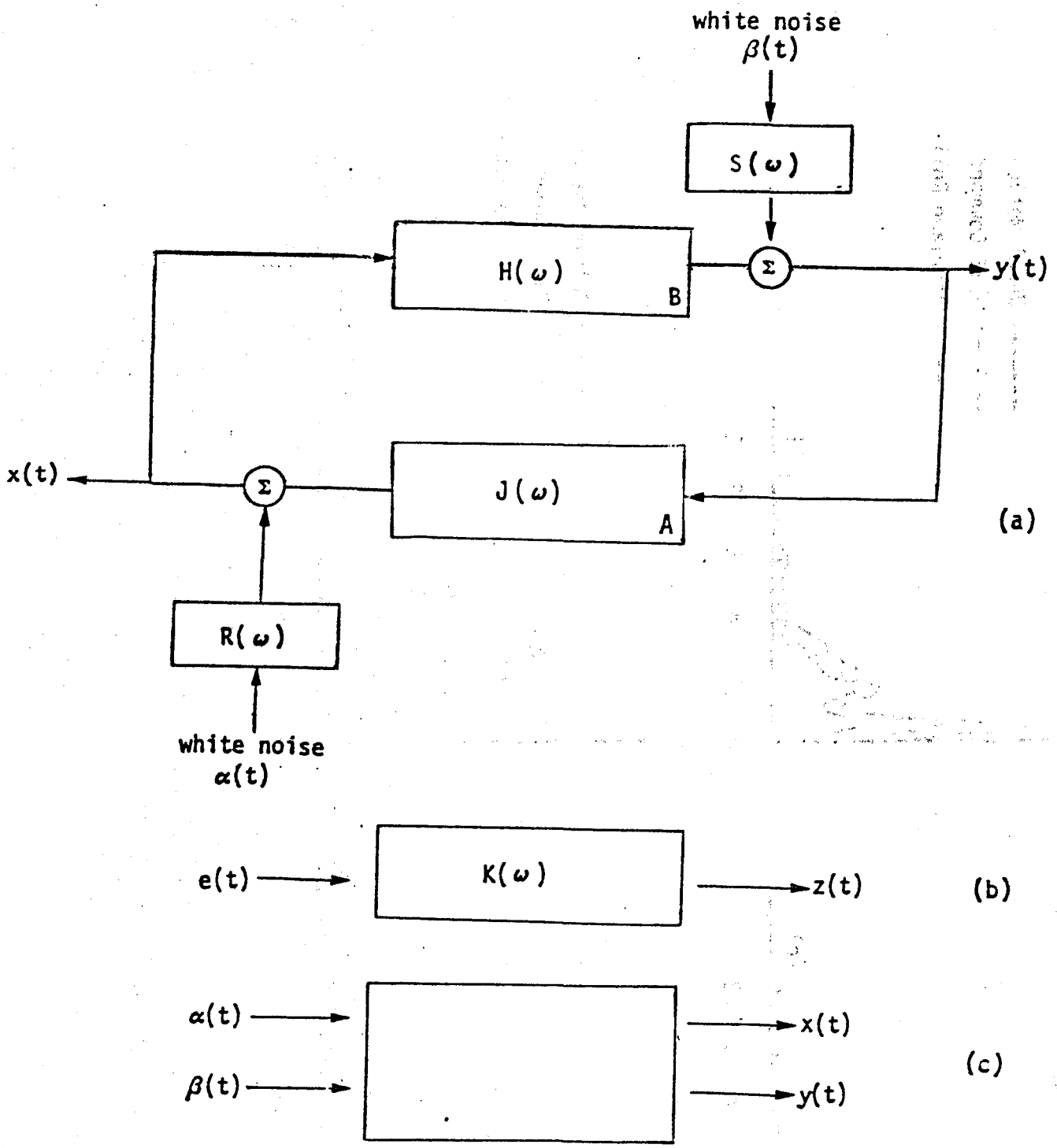

Figure 2 Two Dimensional Open and Closed Loop System Representations

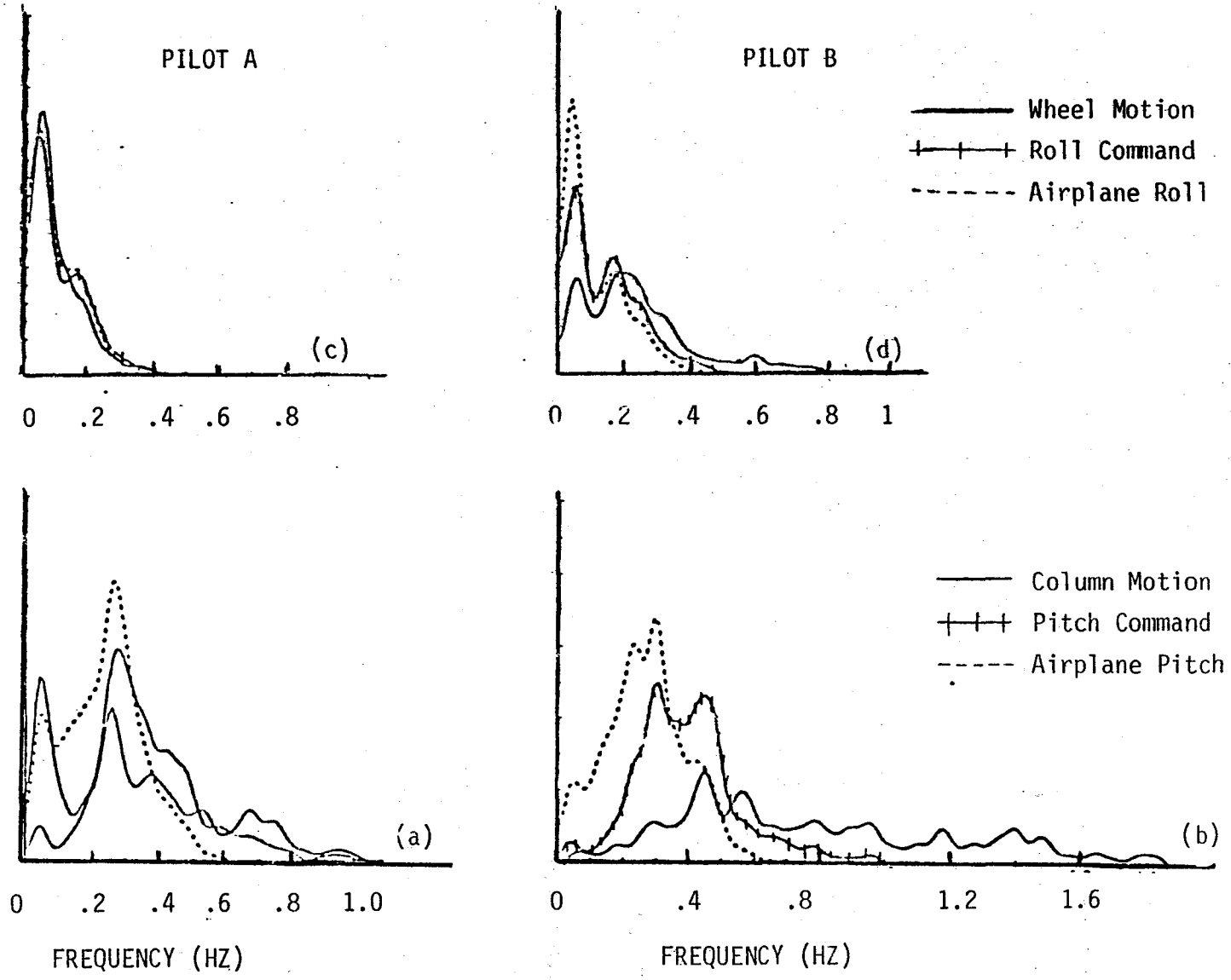

FIGURE 3 Spectral Densities: Roll-related (Top), and Pitch-related (Bottom), for Two Pilots, A (Right), and B (Left)

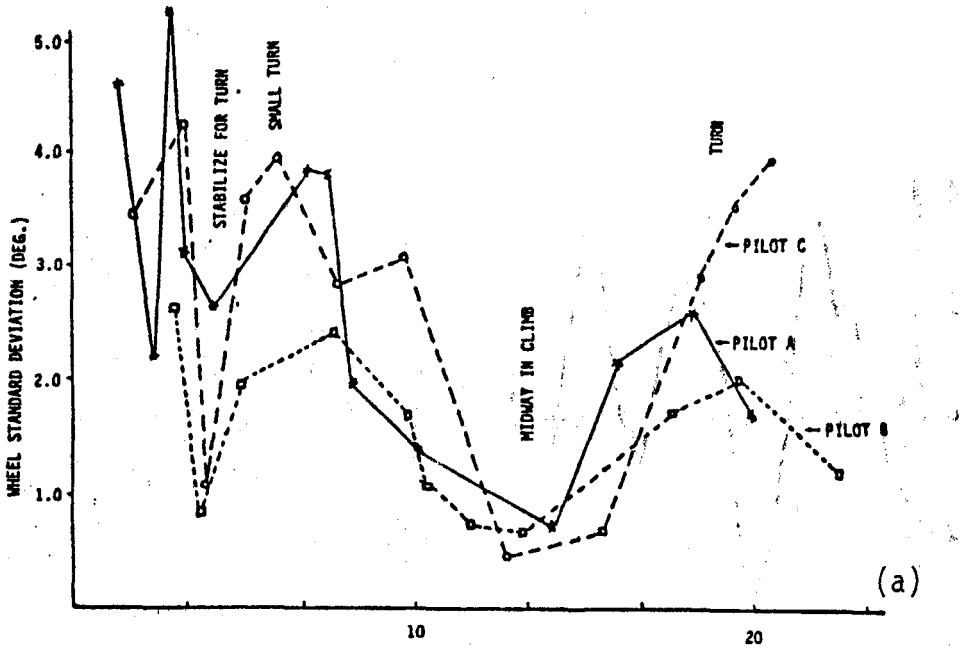

PILOT WHEEL PERFORMANCE

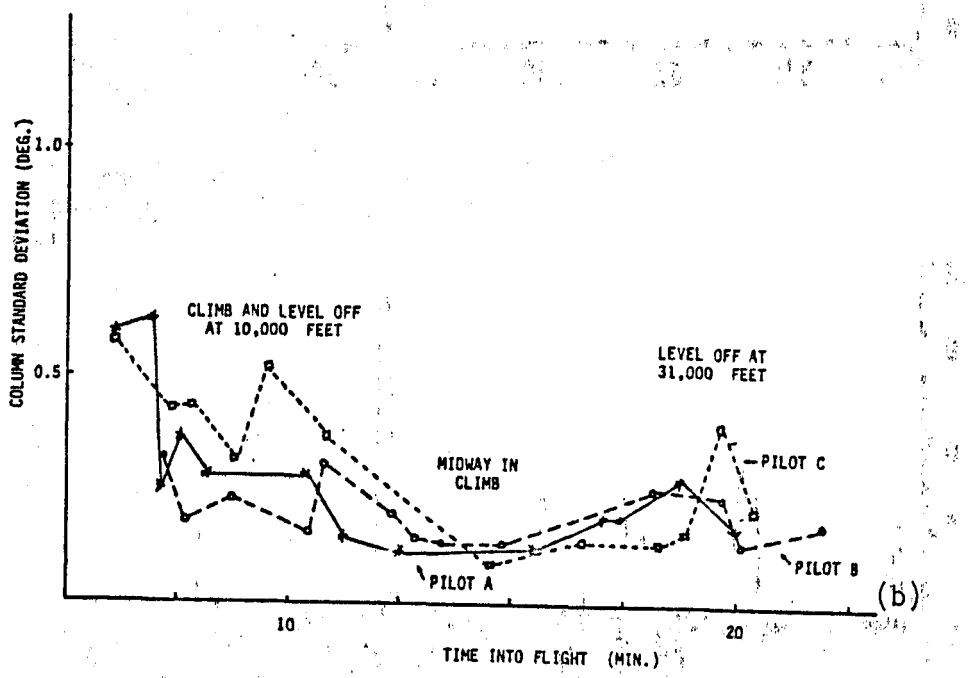

PILOT COLUMN PERFORMANCE

Figure 4 Standard Deviation of Pilot Wheel (a) and Column (b) Performance During Climb Averaged over 1½ minute Intervals -- High Turbulence

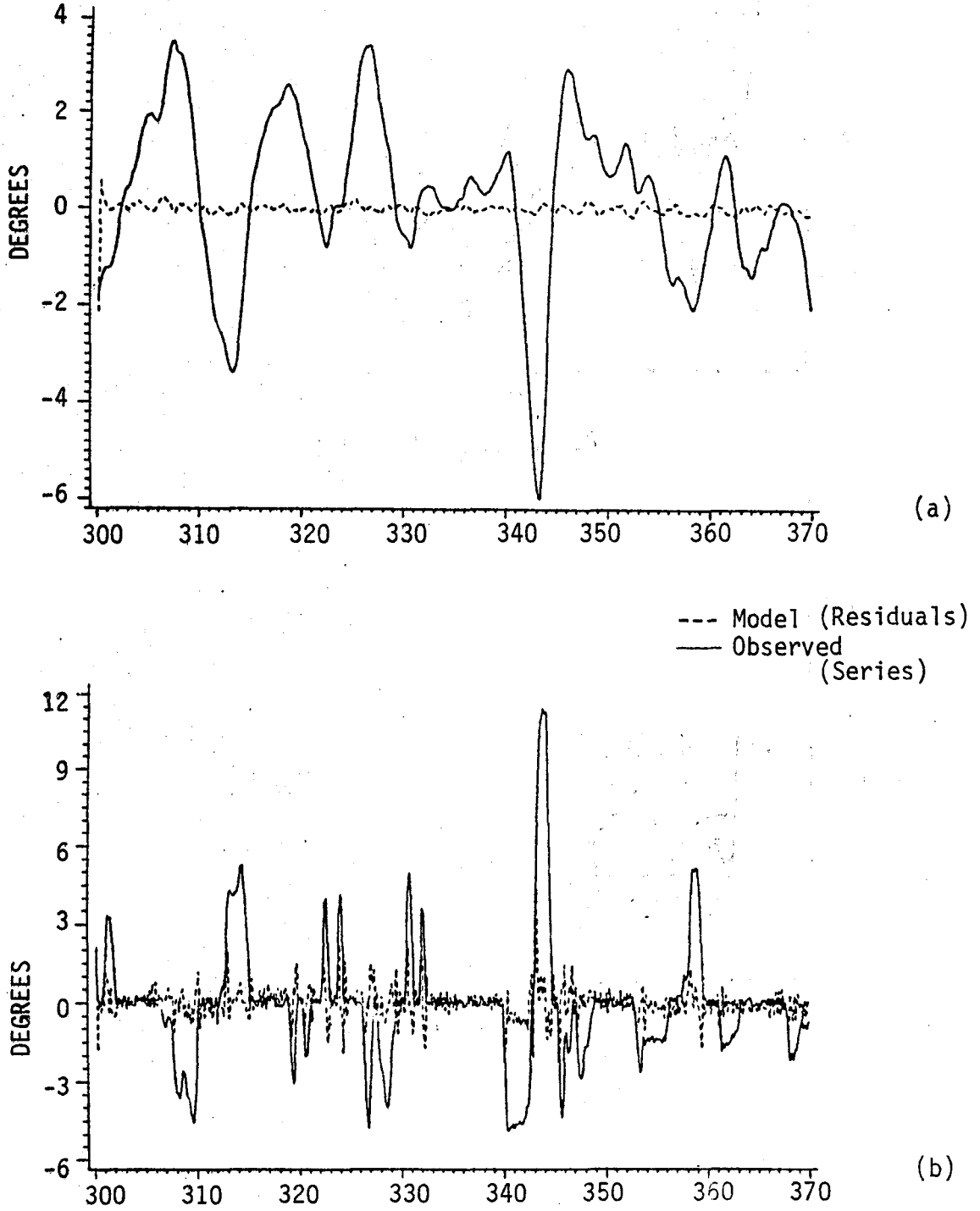

FIGURE 5 Model Residuals superimposed on Roll series (a) and Wheel series (b)

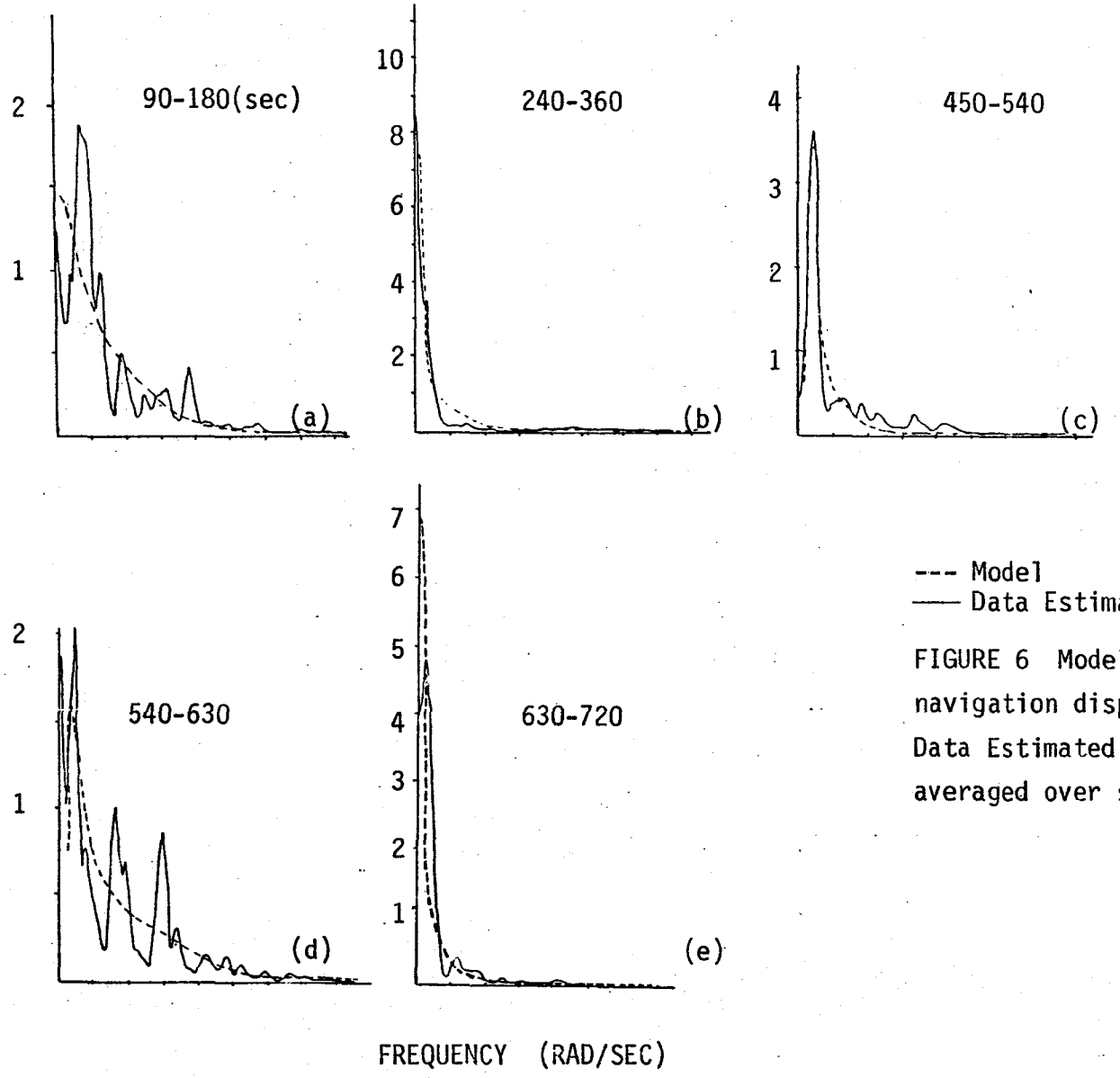

FIGURE 6 Modeled Wheel Spectra, MAP navigation display superimposed on Raw Data Estimated Spectra by Time Into Flight averaged over specified interval.

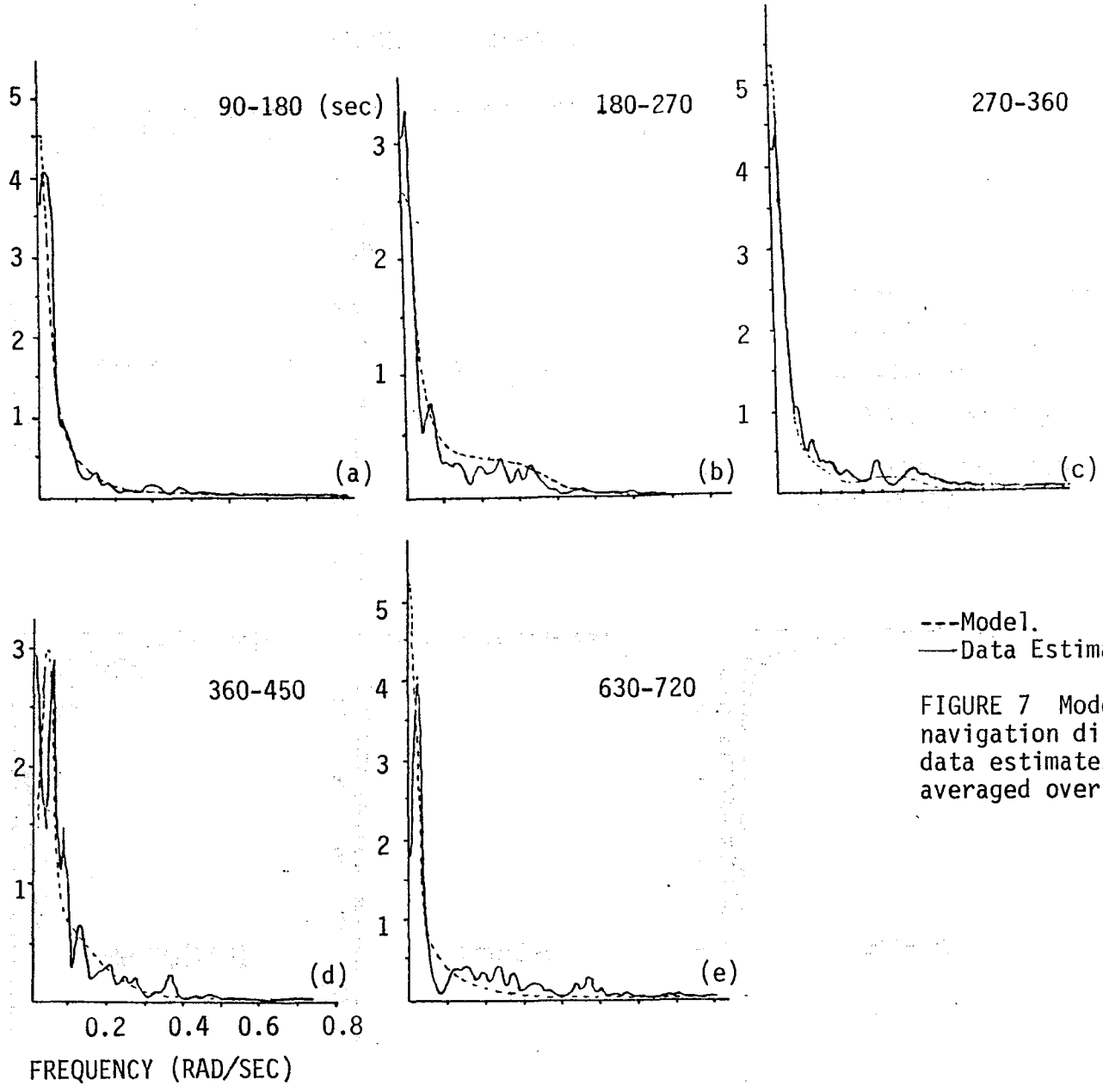

---Model.
——Data Estimate

FIGURE 7 Modeled Wheel Spectra, VOR navigation display superimposed on raw data estimates by time into flight averaged over specified interval

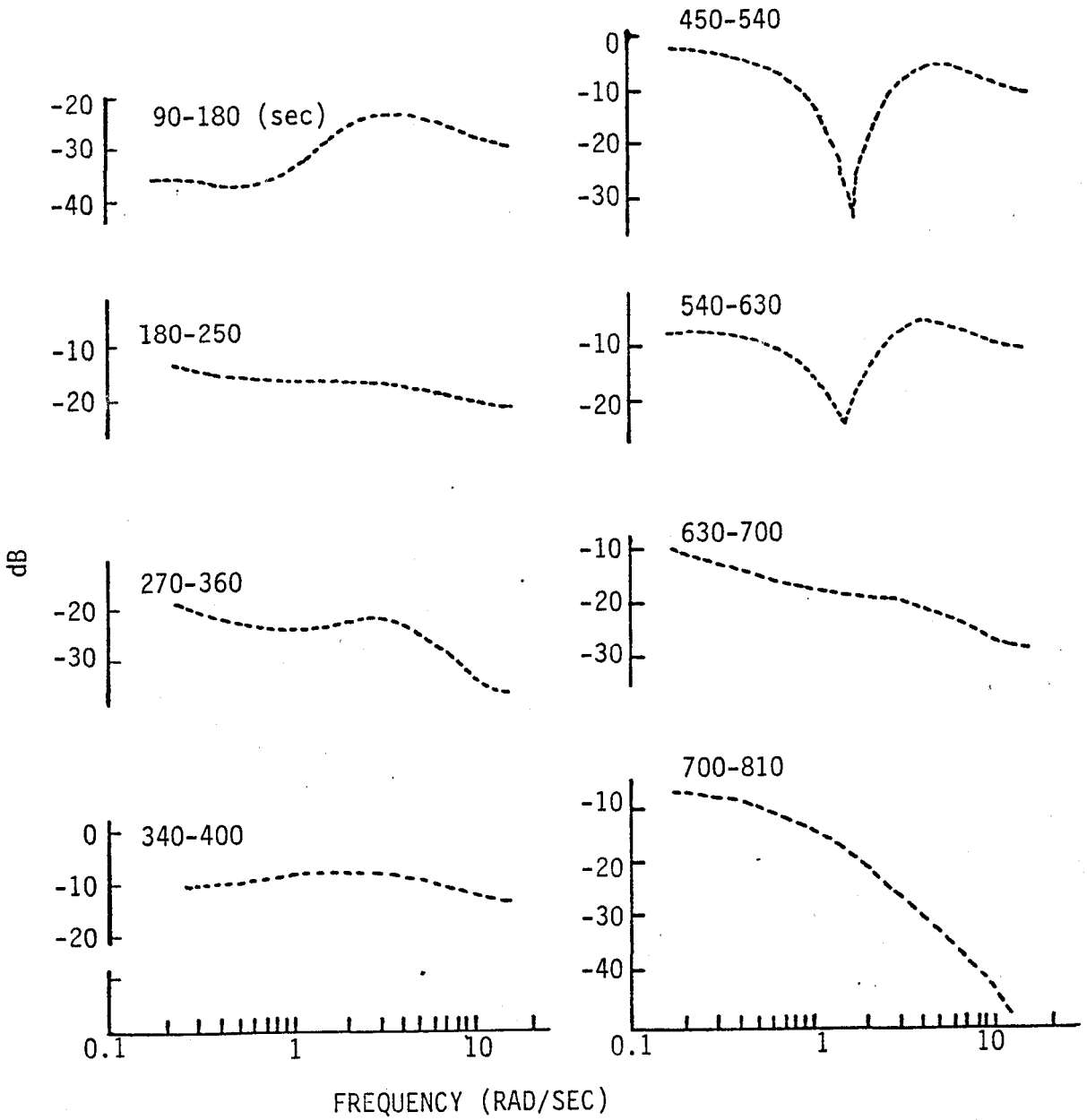

FIGURE 8 Pilot Transfer Functions by Time Into Flight, takeoff to early cruise. Wheel output, Roll input, single pilot: actual flight, MAP navigation mode.

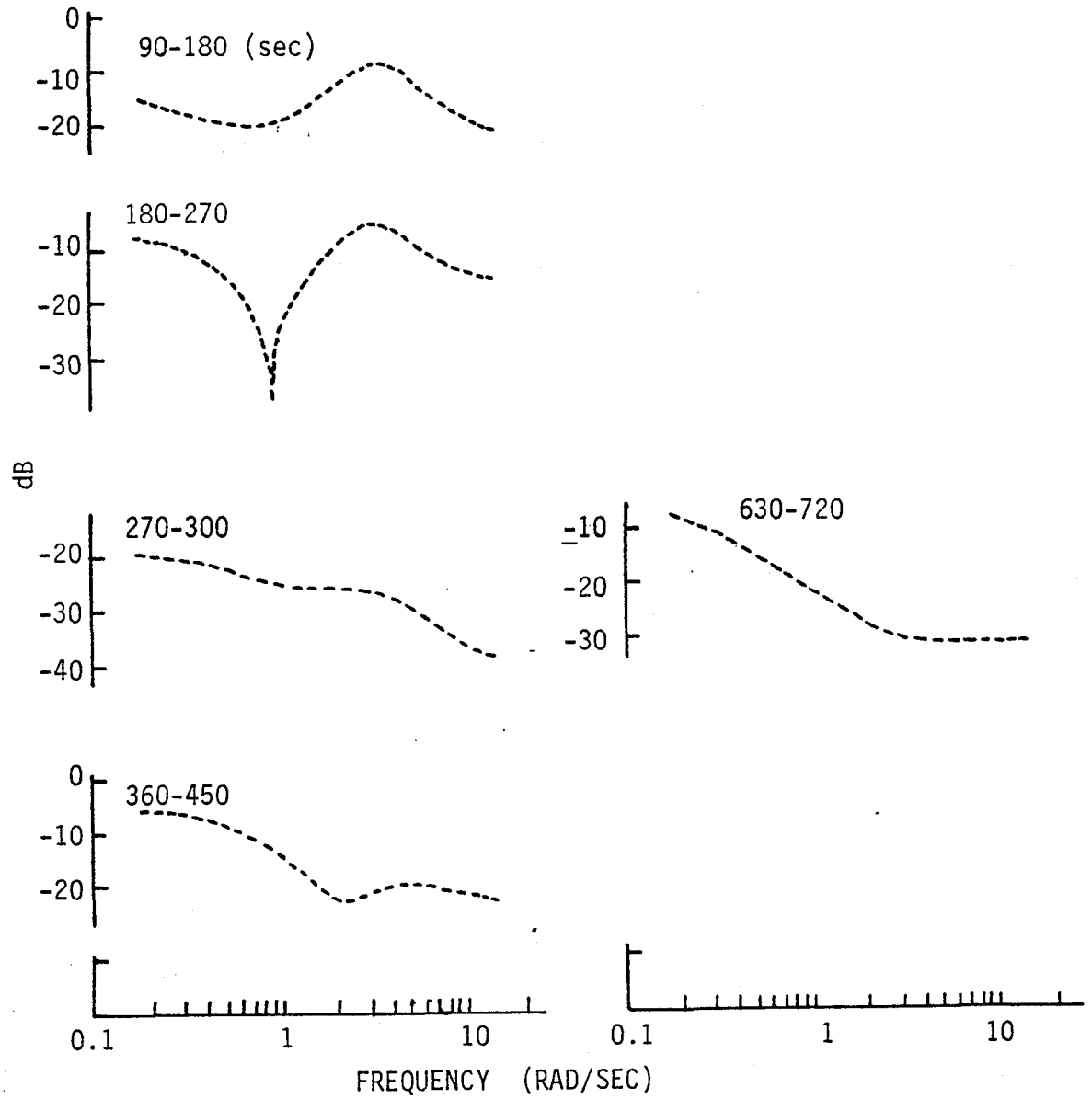

FIGURE 9 Pilot Transfer Functions by Time into Flight, takeoff to cruise, Wheel output, Roll input, Single Pilot: actual flight, VOR navigation mode

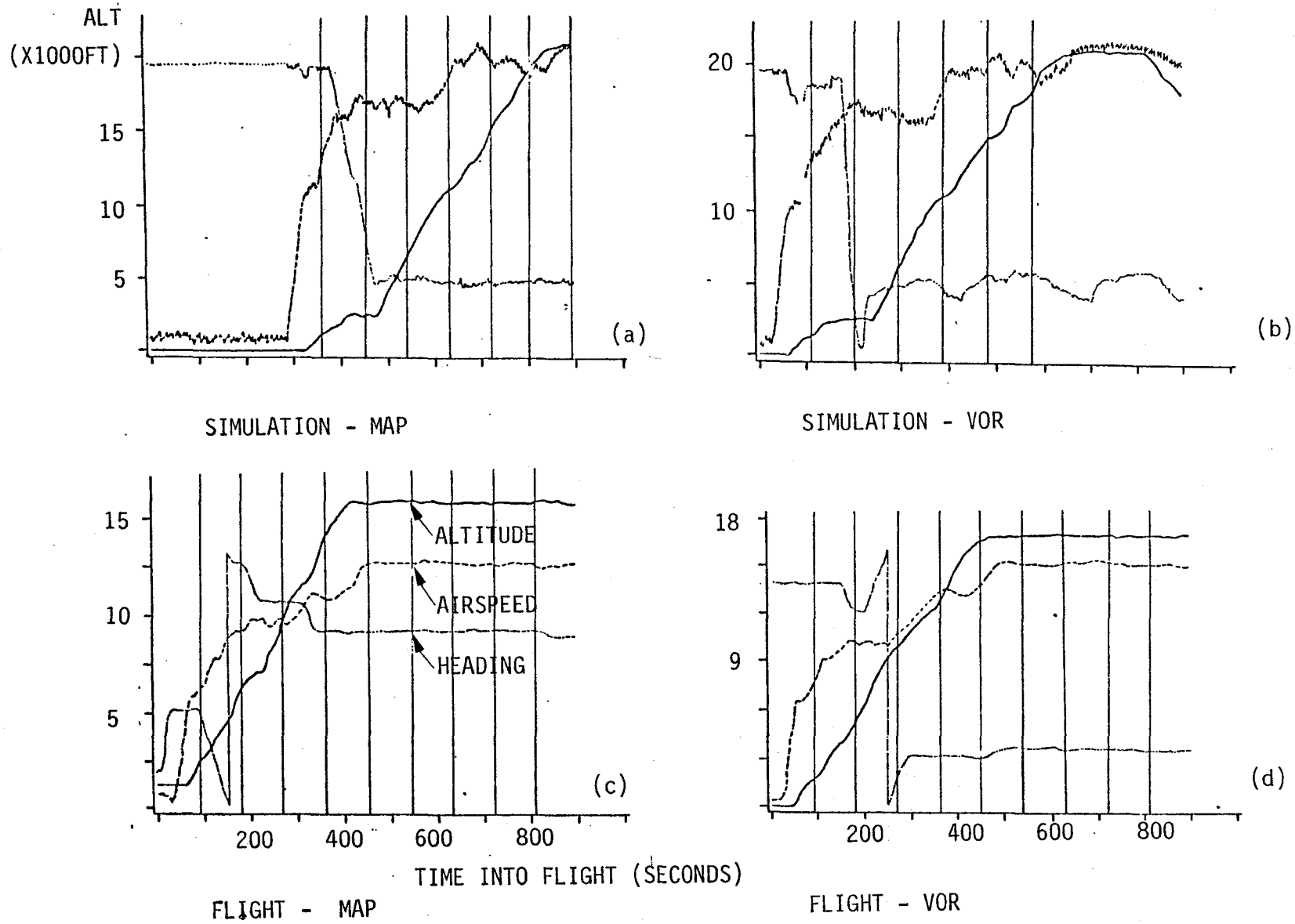

FIGURE 10 Climb Flight Condition Profiles, showing Interval selection. Single pilot, Simulation and flight test, two navigation modes, MAP and VOR.

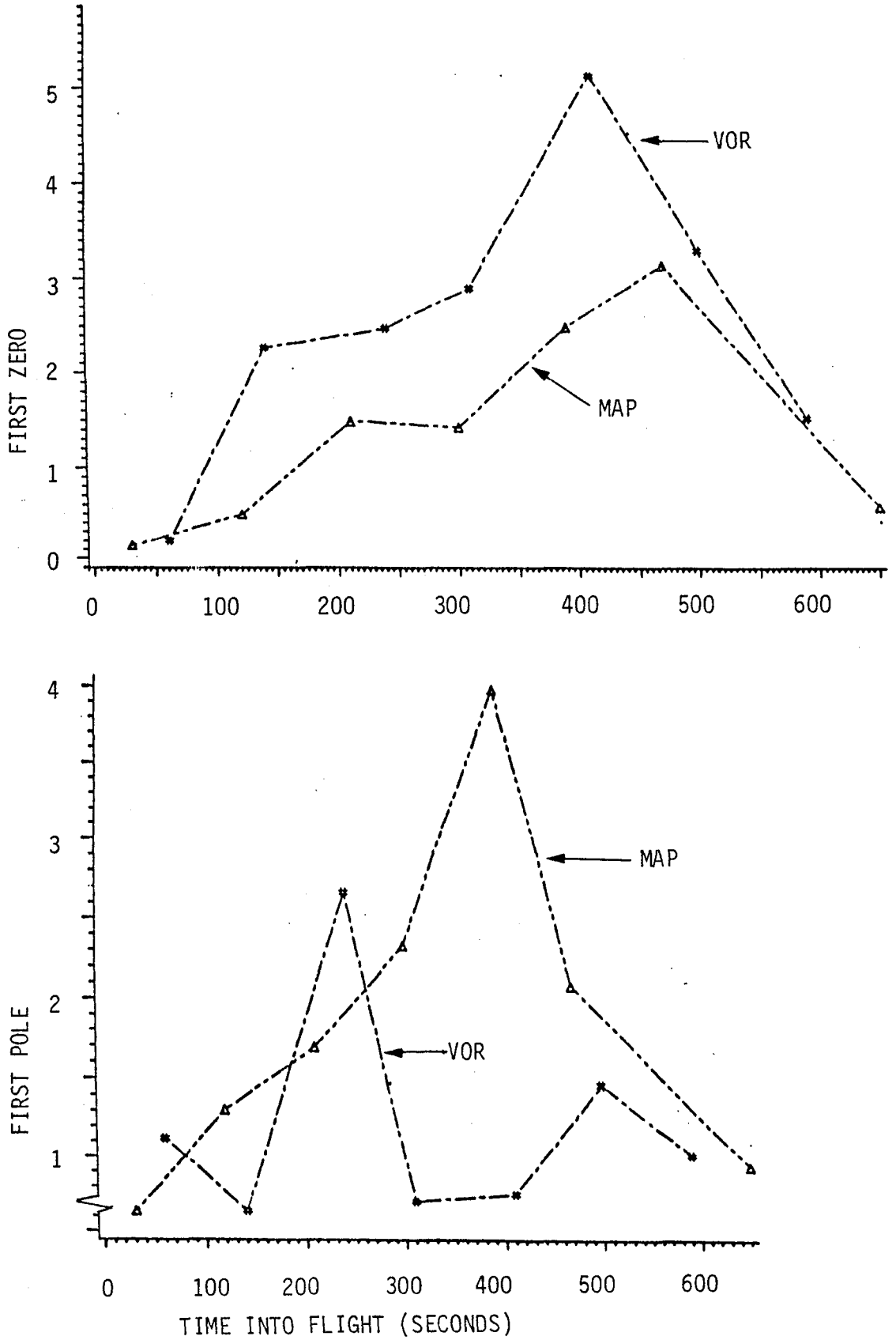

FIGURE 11 Zeroes and Poles of the Pilot Transfer Function, Single Pilot, Simulation, Two Navigation Modes: MAP and VOR

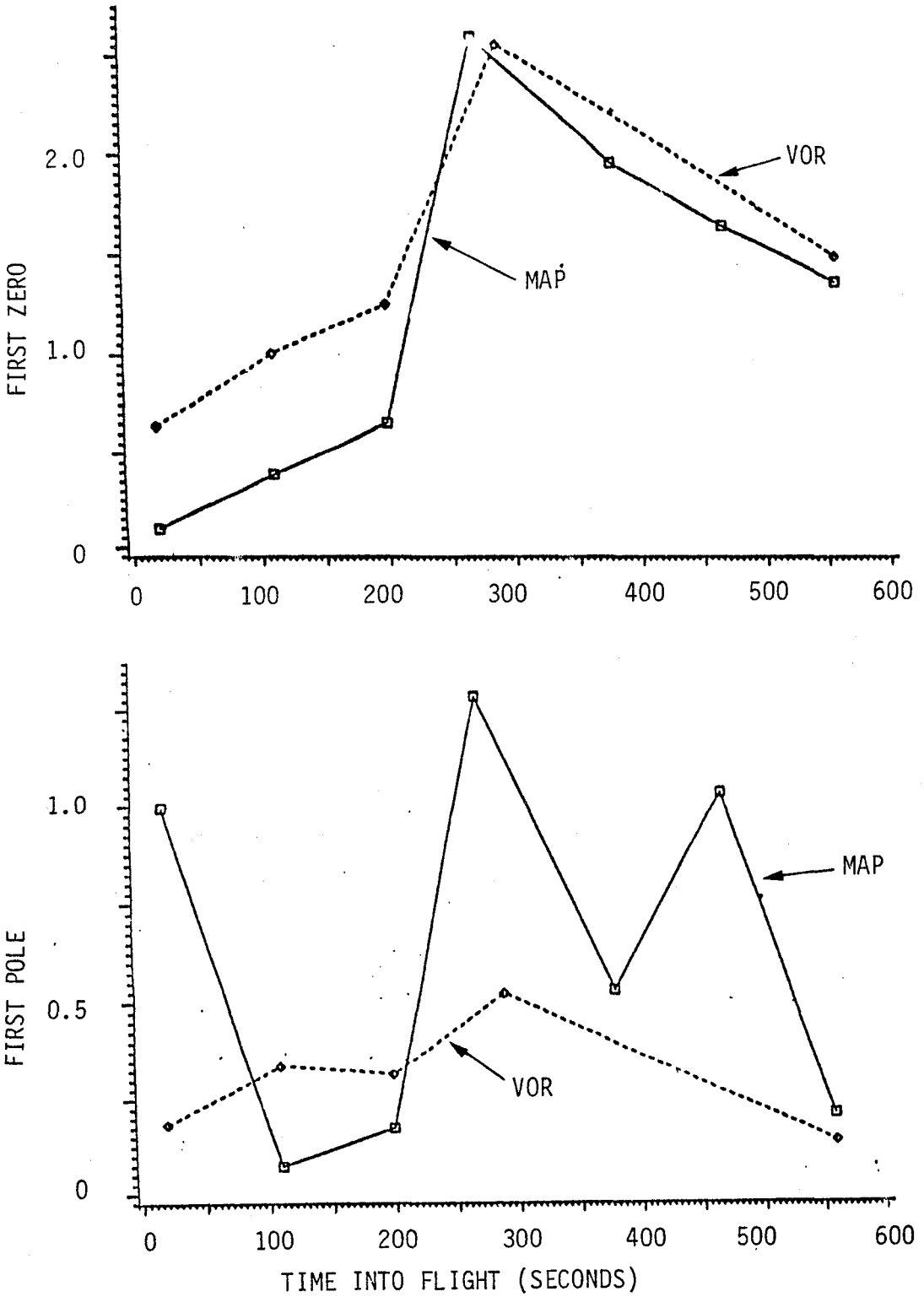

FIGURE 12 Zeroes and Poles of the Pilot Transfer Function, Single Pilot, Actual Flight, Two Navigation Modes, MAP and VOR

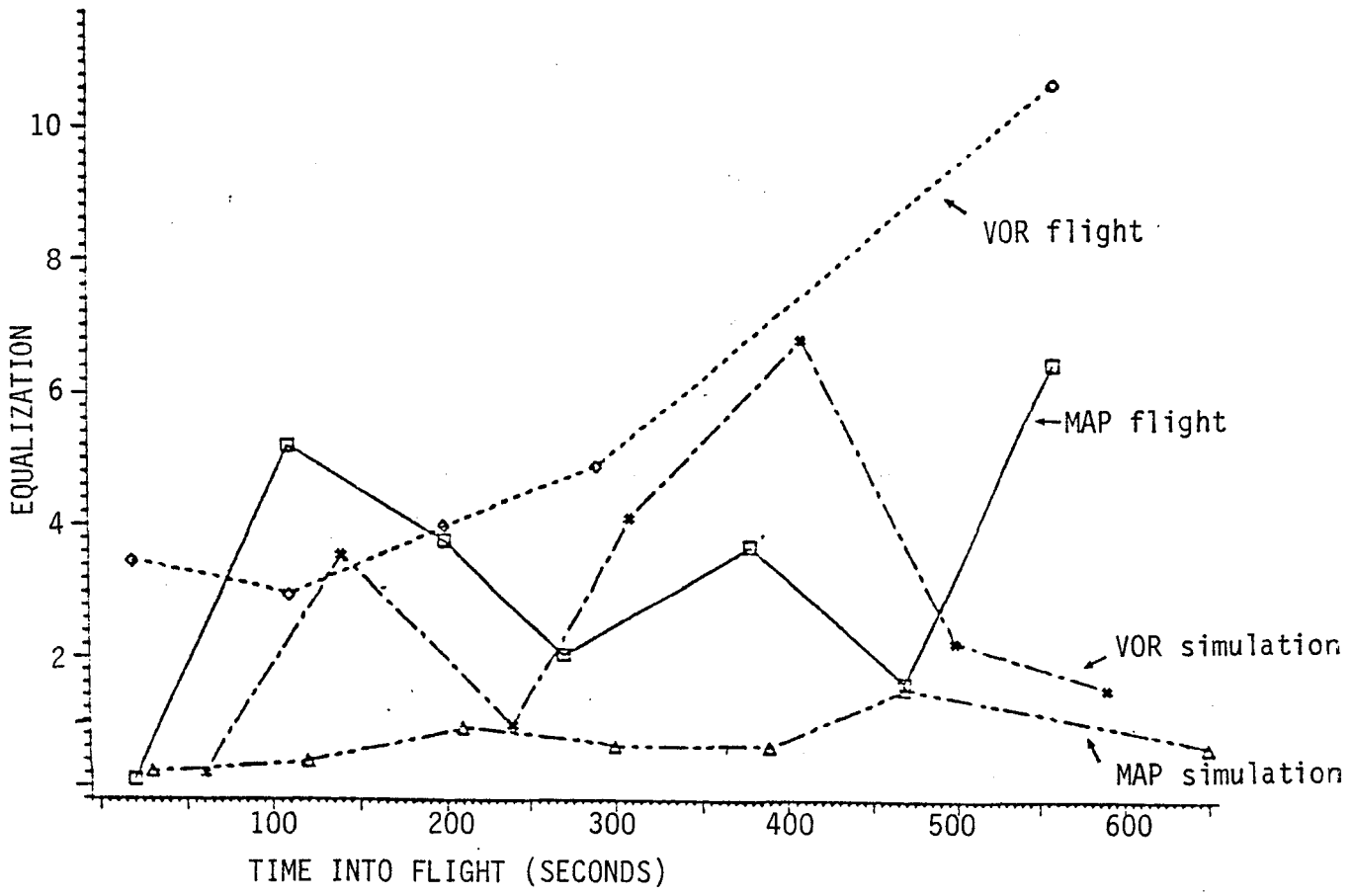

FIGURE 13 Pilot Equalization: First Zero/First Pole
Two navigation modes: MAP and VOR. Single pilot: simulation and flight tests.

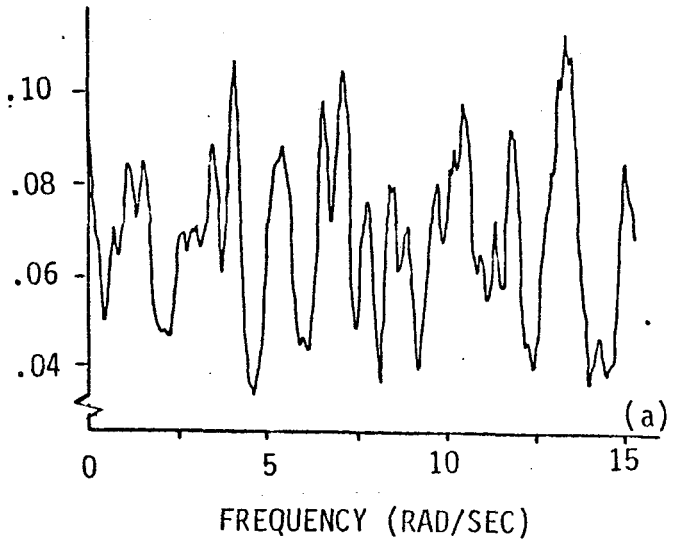

Wheel Residual Spectrum Before and After V_g

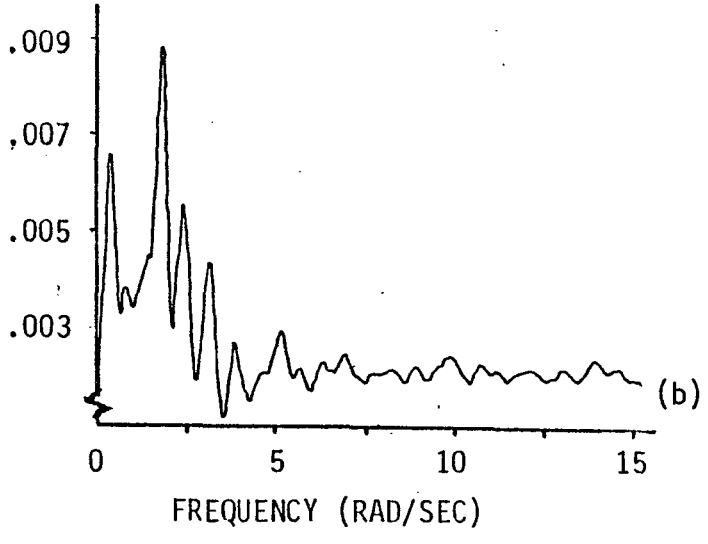

Rate Residual Spectrum Before V_g

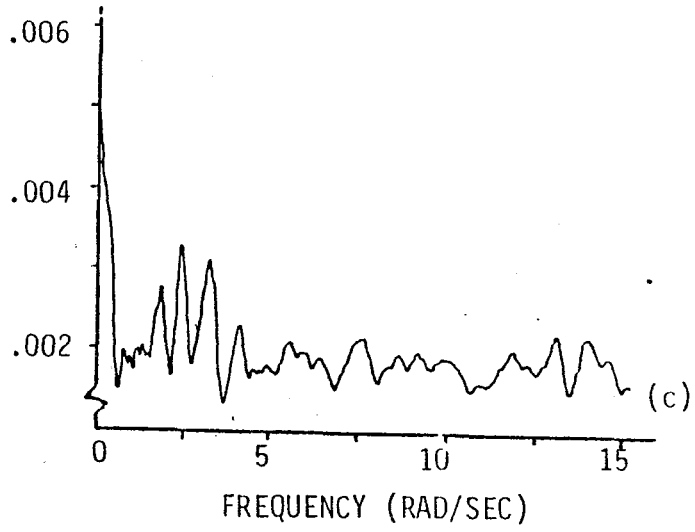

Rate Residual Spectrum After V_g

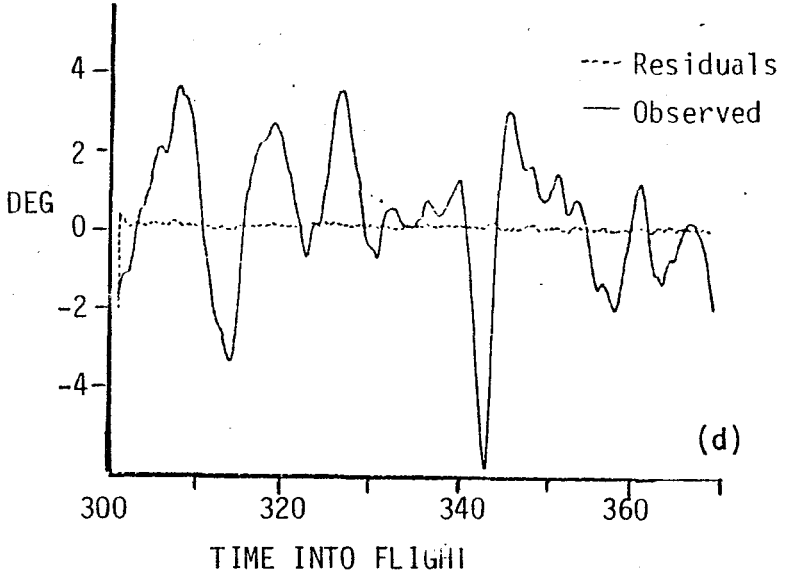

Time History: Model Residuals and Observed Roll Series

FIGURE 14 The Effect of the Lateral Wind Component V_g on the Roll Wheel Model Residuals

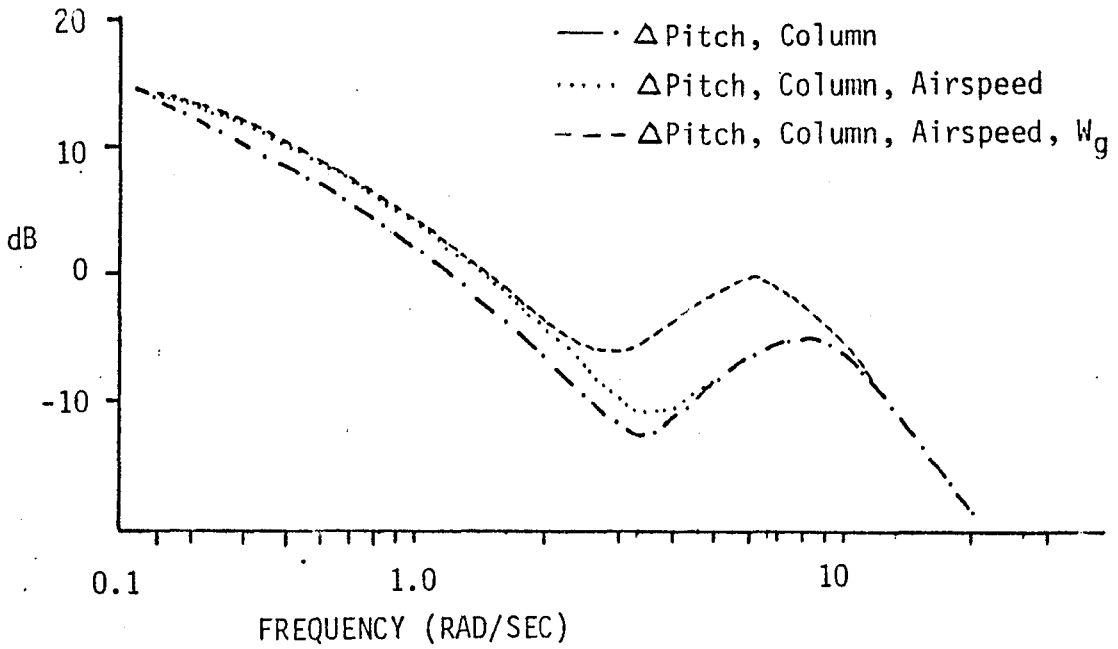

FIGURE 15 Effect of Variable Addition on Test Pilot Transfer Function: Δ Pitch to Column Initially, Airspeed and Vertical Wind, W_g, Added in Sequence